Thermal and Dynamic Mechanical Behavior of Bionanocomposites: Fumed Silica Nanoparticles Dispersed in Poly(vinyl pyrrolidone), Chitosan, and Poly(vinyl alcohol)

Konstantinos Chrissafis,[1] Konstantinos M. Paraskevopoulos,[1] George Z. Papageorgiou,[2] Dimitrios N. Bikiaris[2]

[1]*Solid State Physics Section, Physics Department, Aristotle University of Thessaloniki, GR-541 24 Thessaloniki, Macedonia, Greece*
[2]*Laboratory of Organic Chemical Technology, Department of Chemistry, Aristotle University of Thessaloniki, GR-541 24 Thessaloniki, Macedonia, Greece*

Received 25 February 2008; accepted 20 May 2008
DOI 10.1002/app.28818
Published online 28 July 2008 in Wiley InterScience (www.interscience.wiley.com).

ABSTRACT: Various bionanocomposites were prepared by dispersing fumed silica (SiO_2) nanoparticles in biocompatible polymers like poly(vinyl pyrrolidone) (PVP), chitosan (Chi), or poly(vinyl alcohol) (PVA). For the bionanocomposites preparation, a solvent evaporation method was followed. SEM micrographs verified fine dispersion of silica nanoparticles in all used polymer matrices of composites with low silica content. Sufficient interactions between the functional groups of the polymers and the surface hydroxyl groups of SiO_2 were revealed by FTIR measurements. These interactions favored fine dispersion of silica. Mechanical properties such as tensile strength and Young's modulus substantially increased with increasing the silica content in the bionanocomposites. Thermogravimetric analysis (TGA) showed that the polymer matrices were stabilized against thermal decomposition with the addition of fumed silica due to shielding effect, because for all bionanocomposites the temperature, corresponding to the maximum decomposition rate, progressively shifted to higher values with increasing the silica content. Finally, dynamic thermomechanical analysis (DMA) tests showed that for Chi/SiO_2 and PVA/SiO_2 nanocomposites the temperature of β-relaxation observed in tanδ curves, corresponding to the glass transition temperature T_g, shifted to higher values with increasing the SiO_2 content. This fact indicates that because of the reported interactions, a nanoparticle/matrix interphase was formed in the surroundings of the filler, where the macromolecules showed limited segmental mobility. © 2008 Wiley Periodicals, Inc. J Appl Polym Sci 110: 1739–1749, 2008

Key words: nanocomposites; poly(vinyl pyrrolidone); chitosan; poly(vinyl alcohol); fumed silica nanoparticles; thermal stability

INTRODUCTION

Since 1930s, a wide range of natural minerals have been used as fillers in thermoplastic polymers for various reasons but mainly to reduce the cost of the end products. Traditional fillers like calcium carbonate, talk, mica, silica, alumina, magnesium hydroxide, etc., require high loading amounts to achieve a significantly improved performance. However, the weight increase of the final product is undesirable, especially when compared with the low weight of polymers. To overcome this drawback, during the last few years a new class of mineral-reinforced thermoplastics, termed nanocomposites, has been extensively investigated. In this case, the particulate fillers are in the nanometer size range, preferably less than 100 nm, providing miscibility with the polymer matrix and exploiting unique synergisms between the combined materials.[1–3] Thus, the addition of such nanoparticles in polymeric materials offers many advantages when compared with traditional fillers, forming revolutionary materials. Most of the polymer properties like mechanical strength including stiffness, thermal stability, crystallization rates, and electrical conductivity, even at low filler concentrations, are enhanced. Furthermore, the benefits from nanoparticles incorporation into polymer matrices are the extremely high mechanical properties that the resulting nanocomposites have, compared with neat polymers.

Fumed silica nanoparticles are extensively used in industry as an active filler for the reinforcement of elastomers, as a rheological additive in fluids and as a free flow agent in powders. The size of the primary particle can be controlled by adjusting the synthesis conditions, such as the temperature map in

Correspondence to: D. N. Bikiaris (dbic@chem.auth.gr).

the flame, the flame length, the flow turbulence and velocity, and the ratio of the reactants. Concerning their mechanical properties, fumed silica nanoparticles have very high Young's modulus (71.7 GPa), compressive strength >1.1 GPa, and tensile strength 48.3 MPa while it is a very light material because its density is 2.203 g/cm^3. In our previous studies, SiO_2 nanoparticles were dispersed in different polymer matrices. Study of the formed nanocomposites revealed an increase in their mechanical, thermal properties, and permeability as well as crystallization rates compared to the neat polymers.[4–12] Nowadays, there is an increasing interest especially for nanocomposites based on biocompatible polymers. Excellent examples of such polymer-based nanocomposites applications include bones, cartilage, cobwebs, cuticles, scales, shells, and teeth.[13] PVP is a readily water-soluble polymer as well as in most common polar organic solvents, such as alcohols, amines, acids, and chlorinated hydrocarbons, exhibiting exceptional low toxicity and high biocompatibility. In pharmacy, PVP has a wide spectrum of applications; as a solubilizer, as a crystallization retarder, for detoxification, for reducing the irritant action and toxicity of certain substances, as a tablet binder and coating agent, as a suspension stabilizer, and as a dispersant for pigments in tablet-coating suspensions. Chitosan, poly-D-glucosamine, is a polysaccharide obtained by the deacetylation of chitin (poly-*N*-acetyl-D-glucosamine), and it is a biocompatible polymer with antibacterial and excellent mucoadhesive properties with a variety of applications including additives for cosmetics, biomedical devices, drug nanoparticles, and microcapsule implants for controlled release in drug delivery. Finally, PVA is a hydrophilic polymer containing pendant hydroxyl groups and its aqueous solution can form transparent films. However, it is not soluble in cold water and must be heated at temperatures higher than 90°C. It is a nonionic surfactant, used in pharmaceutical manufacturing as a stabilizing agent, viscosity modifier, and lubricant or as an excipient for tablet formation. PVA hydrogels have gained recently an increasing interest as drug delivery matrices or as pH thermosensitive microcapsules.[14]

PVP, chitosan, and PVA find many applications in biomedical engineering and pharmaceutical industry. Development of nanomaterials based on these polymers is anticipated to be of special interest.[15,16] Thus, the aim of this study was to prepare biocompatible organic/inorganic hybrids by dispersing fumed silica nanoparticles in PVP, chitosan, or PVA and to evaluate the effect of SiO_2 content on the morphology and the key properties of such bionanocomposites, meaning, mechanical and dynamic thermal mechanical properties as well as thermal stability. Because all these polymers are biocompatible, the prepared nanocomposites in this study are referred to as bionanocomposites.

EXPERIMENTAL

Materials

PVP type Kollidon K30 with a molecular weight of 50,000–55,000, T_g = 167°C (DSC analysis), moisture content 1.95% (TGA analysis), and bulk density 0.410 g/cm^3 was obtained from BASF (Ludwigshafen, Germany). Chitosan with a low molecular mass and viscosity 170–200 cP (1 wt % in 1% acetic acid, Brookfield), 75–85% deacetylated was supplied from Aldrich chemicals (Steinheim, Germany). PVA was supplied from DuPont Co under the trade name Elvanol® 70–30 having a mole percent hydrolysis of acetate groups 98.5–99.2 and viscosity 25–30 cP (4% water solution). Fumed silica (SiO_2) nanoparticles used for the nanocomposites preparation were supplied by Degussa AG (Hanau, Germany) under the trade name AEROSIL® 200. The average primary particle size was 12 nm, the specific surface area was 200 m^2/g, and the SiO_2 content was >99.8%. All other materials and reagents were of analytical grade of purity.

Nanocomposites preparation

Chitosan/fumed silica nanocomposites were prepared by dissolving the proper amount of chitosan in water containing 2 wt % acetic acid, whereas fumed silica was dispersed in water under ultrasonication producing a slightly viscous transparent dispersion. Upon addition to the chitosan solution, the final viscosity was increased but the solution remained transparent. The solutions were homogenized under ultrasonication and maintained at 60°C for water evaporation.

PVP nanocomposites were prepared by dissolving the appropriate quantities of the dry substance in water at room temperature. The solutions were mixed with silica dispersion, subsequently ultrasonicated for 20 min, and then the solvent was fully evaporated at 60°C.

Films of PVA/SiO_2 nanocomposites were prepared by a simple casting procedure from aqueous solutions. PVA was dissolved at 95°C under magnetic stirring and silica dispersion in water, prepared as described earlier, was gradually added under ultrasonication. The solution was maintained at 60°C for water evaporation.

FTIR spectroscopy

FTIR spectra were obtained using a Perkin–Elmer FTIR spectrometer, model Spectrum 1000 using KBr

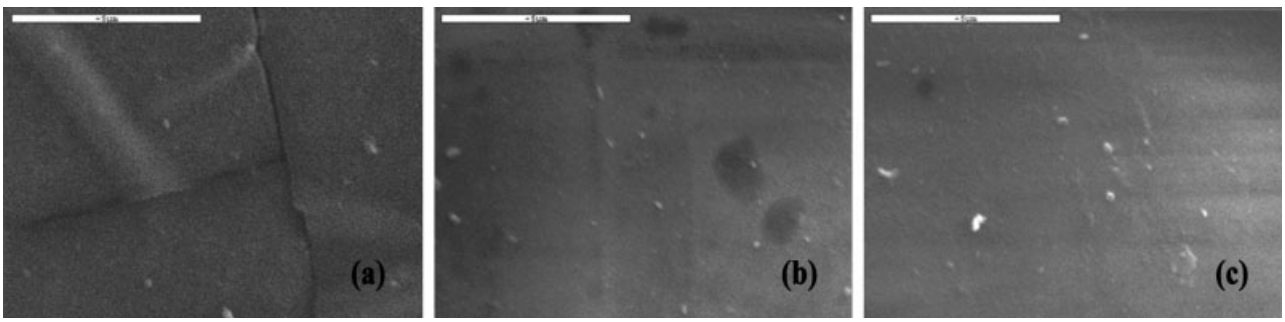

Figure 1 SEM micrographs of PVA/SiO_2 nanocomposites containing (a) 2.5, (b) 5, and (c) 15 wt % SiO_2.

tablets. All samples were dried first at 120°C under reduced pressure for 24 h prior to collect their spectra. The resolution for each spectrum was 2 cm^{-1}, and the number of coadded scans was 64. The spectra presented were baseline corrected and converted to the absorbance mode.

Scanning electron microscopy

SEM study was carried out using a JEOL JMS-840A scanning microscope equipped with an energy-dispersive X-ray (EDX) Oxford ISIS 300 microanalytical system. For this purpose, fractured surfaces as well as thin films were used. All the studied surfaces were coated with carbon black to avoid charging under the electron beam.

Mechanical properties

Measurements of tensile mechanical properties of the prepared bionanocomposites were performed on an Instron 3344 dynamometer in accordance with ASTM D638 using a crosshead speed of 50 mm/min. Relatively, thin films of about 350 ± 25 μm were prepared by film casting method. From these films, dumb-bell shaped tensile-test specimens (central portions 5 × 0.5 mm thick, 22-mm gauge length) were cut in a Wallace cutting press and conditioned at 25°C and 55–60% relative humidity for 48 h. The values of Young's modulus, elongation at break, and tensile strength were determined from the respective stress–strain curves. At least, five specimens were tested for each sample and the average values together with the corresponding standard deviations are reported.

Differential scanning calorimetry

A Setaram DSC141 differential scanning calorimeter (DSC), calibrated with indium and zinc standards, was used for thermal analysis. Samples of about 10 mg were used for each test, placed in an aluminum pan, and heated up to 200°C for PVP/SiO_2 and Chi/SiO_2 nanocomposites and up to 250°C for PVA/SiO_2 nanocomposites at a heating rate of 20°C/min. The glass transition temperature (T_g) of the amorphous polymers and the melting temperature of PVA (T_m) were measured. All samples were dried first at 120°C under reduced pressure for 24 h.

Thermogravimetric analysis

Thermogravimetric analysis (TGA) was carried out with a TG-DTA Setaram Setsys 16/18. Samples (11 ± 0.5 mg) were placed in an alumina crucibles. An empty alumina crucible was used as reference. Samples were heated from ambient temperature to 500°C in a 50 mL/min flow of N_2 with a heating rate of 10°C/min. Continuous records of sample temperature, sample weight, its first derivative, and heat flow were taken. All measurements were repeated at least three times.

Dynamic mechanical analysis

The dynamic thermomechanical properties of the nanocomposites were measured with a Perkin–Elmer Dynamic Mechanical Analyzer (model Diamond). The bending method was used at a frequency of 1 Hz in the temperature range of 30–200°C depending on the nanocomposite. The heating rate was 3°C/min. Testing was performed using rectangular bars measuring ~ 30 mm × 10 mm × 0.5 mm, which were prepared as described earlier. The exact dimensions of each sample were measured before the scan.

RESULTS AND DISCUSSION

Morphological characterization

After solvent evaporation, the prepared films of bionanocomposites were transparent. This fact indicated that fumed silica was fine dispersed in all used matrices. However, fine dispersion of SiO_2 nanoparticles in polymer matrices was evaluated studying the respective SEM micrographs. Only at load content higher than 5 wt %, existence of some agglomerates of silica particles with sizes in the range of 100–200 nm was observed (Fig. 1).

Formation of agglomerates of nanoparticles is the most common problem in nanocomposites preparation. In this work, formation of agglomerates was the result of the interactions occurring between the silica nanoparticles themselves, because they contain a lot of surface hydroxyl groups.

As was concluded from the FTIR spectroscopy studies, the interactions taking place between the carbonyl groups of PVP and the hydroxyl groups of SiO_2 are weak. Most probably, in such a case, interactions between nanoparticles themselves dominated. On the contrary, the amino groups of chitosan and the hydroxyl groups of PVA show much stronger interactions with silica (Fig. 2). For the studied PVP/SiO_2 nanocomposites only shifts in the wavenumber of the carbonyl groups of PVP to slightly higher values, i.e., from 1660 to 1662 cm^{-1}, were observed [Fig. 2(a)]. Because the difference is very small, only weak interactions could be supposed. In relative studies, it was reported that in the best case, and if the polymer filler weight ratio is appropriate, interactions might result in formation of a PVP monolayer on the silica surface.[17,18] On the other hand, significant shifts are recorded in the corresponding positions of the absorbance peaks of Chi/SiO_2 and PVA/SiO_2 nanocomposites [Fig. 2(b,c)]. In the chitosan spectrum, the peaks at 3418 and 3271 cm^{-1} are attributed to the —OH and —NH_2 groups, respectively, whereas other characteristic absorbencies are that of >*N*—H group (in-plane bending) which are recorded at 1562 cm^{-1} [Fig. 2(b)]. In the chitosan/SiO_2 nanocomposites, these bands are shifted to 3421 and 3262 cm^{-1}, respectively, for nanocomposites containing up to 10 wt % of SiO_2. Additionally, the absorption band at 1562 cm^{-1} was shifted to 1565 cm^{-1} indicating that the —NH_2 groups of chitosan are involved in grafting reactions. In PVA/SiO_2 spectra, there is a shift of the peak associated with >C—OH bond stretching to lower wavenumbers, from 1095 to 1089 cm^{-1}, indicating that the hydroxyl groups of PVA participate in such hydrogen bonds [Fig. 2(c)]. Furthermore, in the range of 3100–3700 cm^{-1}, the peaks recorded for neat PVA at 3485 and 3296 cm^{-1} were shifted [Fig. 2(c)]; the first one shifted to higher wavenumbers between 3498 and 3536 cm^{-1}, depending on the silica amount, whereas the second one shifted downward from 3294 to 3287 cm^{-1}. This ability of PVA to form hydrogen bonds with surface hydroxyl groups of SiO_2 is schematically illustrated in Figure 3, and it has also been recently reported for the case of different kind of nanoparticles having such reactive groups.[19] Similar interactions are taking place between amine groups of chitosan and SiO_2 hydroxyl groups.[20] From the earlier study, it was concluded that the tendency of hydrogen bond formation was more pronounced in the case of Chi/SiO_2 and PVA/SiO_2 than for the PVP/SiO_2 bionanocomposites.

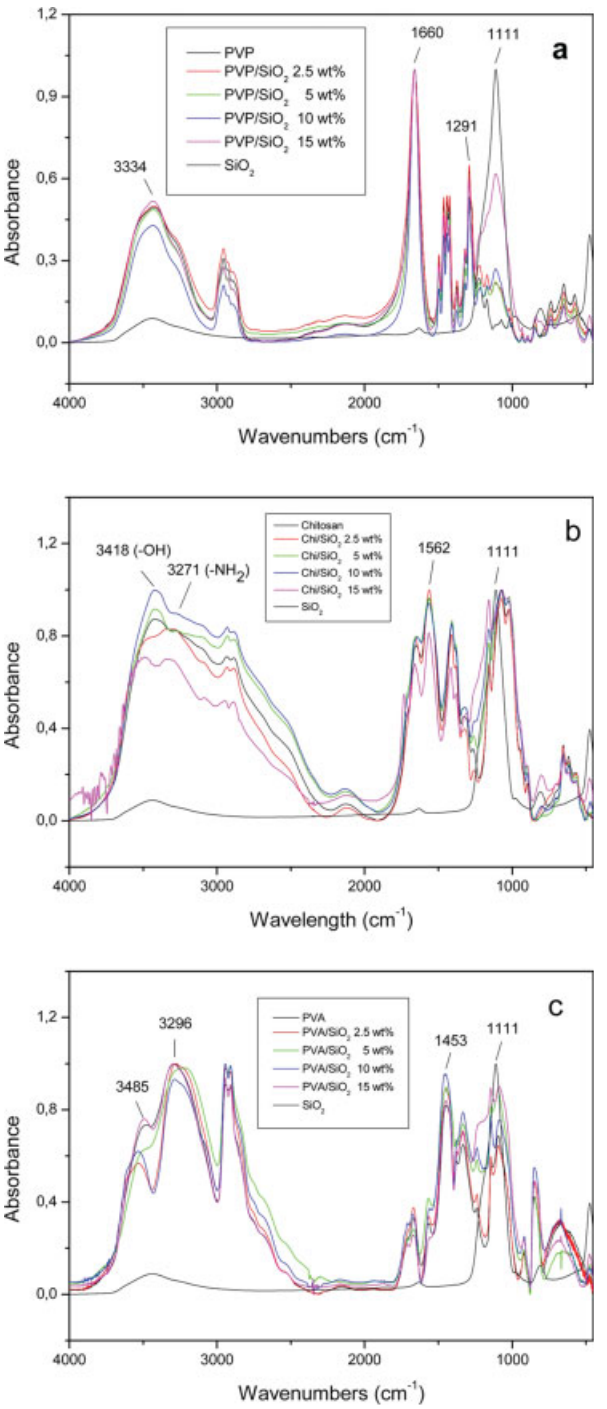

Figure 2 FTIR spectra of (a) PVP/SiO_2, (b) Chi/SiO_2 and (c) PVA/SiO_2 nanocomposites bionanocomposites. [Color figure can be viewed in the online issue, which is available at www.interscience.wiley.com.]

Mechanical properties and dynamic mechanical analysis

For all nanocomposites, mechanical properties were measured and results are presented in Table I, except those of PVP/SiO_2 bionanocomposites, which even at high silica loading (15 wt %) remain very brittle and was not possible to prepare tensile test

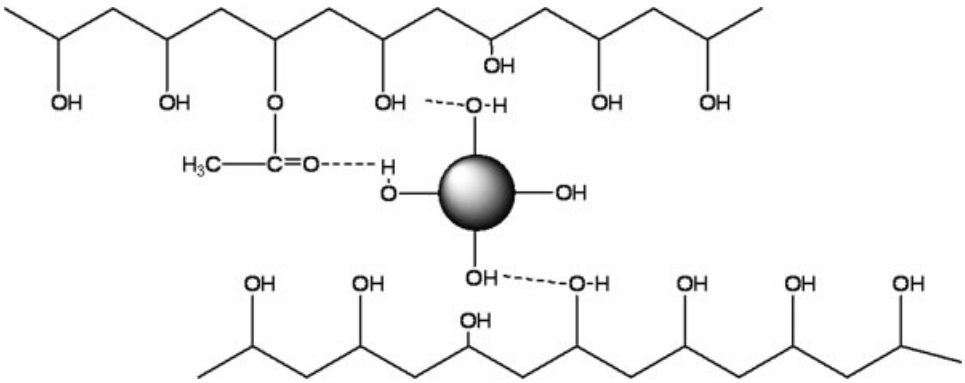

Figure 3 Schematic representation of the evolved interactions between PVA and SiO_2 nanoparticles.

specimens. As can be seen, for all the materials there was a substantial increase in tensile strength and Young's modulus after the incorporation of silica nanoparticles. It should be noted that for these nanocomposites both the above mechanical properties increased with increasing the SiO_2 content. Usually, in nanocomposites containing SiO_2 an optimum for the mechanical properties is achieved for 2.5–5 wt % nanoparticles load. For higher filler amount a decrease is observed in tensile strength.[3–5] This is due to the increased tendency of nanoparticles to create agglomerates. However, for the nanocomposites of this work continuous increase of the tensile strength was observed with increasing the nanoparticles content up to 15 wt %. For samples containing 15 wt % of SiO_2, which is considered a very high loading, the highest values for tensile strength were achieved being 78 and 68 MPa for Chi/SiO_2 and PVA/SiO_2, respectively. Young's modulus showed an increase of up to 50% by the addition of 10 or 15 wt % SiO_2 in the case of Chi/SiO_2 nanocomposites. This high increase of mechanical properties should be attributed to the increased interactions that take place between the surface hydroxyl groups of SiO_2 and the reactive groups of PVA and chitosan, as was already verified by FTIR spectroscopy. The effect of SiO_2 nanoparticles on elongation at break was negligible in Chi/SiO_2 nanocomposites, because they were brittle materials. However, in the case of PVA/SiO_2 nanocomposites elongation at break reduced by increasing the SiO_2 content.

The increased stiffness of the studied nanocomposites was also verified from dynamic thermomechanical analysis (DMA) measurements. The storage

TABLE I
Mechanical and Thermal Properties of the Prepared Bionanocomposites[a]

SiO_2 (wt %)	Tensile strength (MPa)	Young's modulus (MPa)	Elongation at break (%)	T_g[b] (°C)	T_g[c] (°C)	T_m (°C)
PVP/SiO_2 nanocomposites						
0	–	–	–	163	165	–
2.5	–	–	–	163	165	–
5.0	–	–	–	164	166	–
10.0	–	–	–	164	167	–
15.0	–	–	–	165	166	–
Chisotsan/SiO_2 nanocomposites						
0	51 ± 5	2,200 ± 220	5 ± 1.3	137	137	–
2.5	67 ± 7	2,770 ± 310	5.6 ± 1.7	139	141	–
5.0	69 ± 4	2,800 ± 270	7.1 ± 2.1	144	145	–
10.0	74 ± 5	3,010 ± 400	6.5 ± 2.2	144	146	–
15.0	78 ± 6	3,000 ± 360	7.2 ± 2.2	150	152	–
PVA/SiO_2 nanocomposites						
0	51 ± 3	926 ± 30	520 ± 90	51	53	226
2.5	60 ± 8	897 ± 42	423 ± 80	55	58	227
5.0	62 ± 6	940 ± 35	375 ± 110	59	62	227
10.0	64 ± 5	966 ± 42	355 ± 60	66	67	228
15.0	68 ± 6	1078 ± 40	294 ± 45	74	73	229

[a] For PVP/SiO_2 nanocomposites due to the brittleness of the prepared films, it was not possible to measure their tensile properties.
[b] Values measured from DSC thermograms.
[c] Values measured from DMA data.

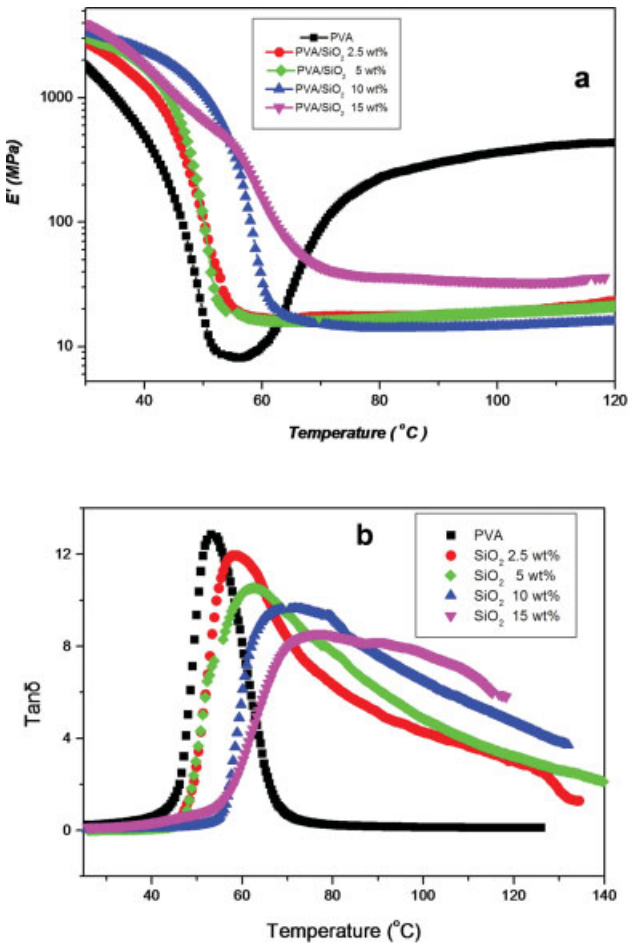

Figure 4 Dynamic mechanical measurements of PVA/SiO_2 nanocomposites as function of temperature. (a) Storage modulus and (b) tan δ. [Color figure can be viewed in the online issue, which is available at www.interscience.wiley.com.]

modulus of all nanocomposites was higher than the corresponding of neat polymers. Figure 4 demonstrates representative storage modulus and tan δ curves of PVA/SiO_2 nanocomposites, as recorded during dynamic mechanical analysis in the temperature range of 25–150°C. As can be seen from the storage modulus (E') curves at low temperatures (25–50°C), all PVA/SiO_2 nanocomposites have higher E' values than neat PVA [Fig. 4(a)]. Furthermore, at 25°C storage modulus of PVA nanocomposite containing 15 wt % SiO_2 is almost double that of neat PVA. Loss modulus (E'') at this temperature range showed a peak. Both position and intensity of the peak varied with varying filler content in the nanocomposites. From the variation of the ratio E''/E' (the so-called tan δ) with temperature, relaxations of the materials can be determined a-relaxation, which in fact corresponds to the glass transition, appears as a peak in tan δ versus temperature plots. The observed increase of the glass transition temperature (T_g) directly reflects the reduction of segmental mobility of polymer chains and the increase in stiffness of the composites as a result of incorporation of SiO_2 and evolution of interactions with the respective polymer matrices. As can be seen from Figure 4(b), PVA exhibited a glass transition temperature of 53.3°C. The T_g values for the nanocomposites increased with increasing the silica content. More specifically, the T_g became 58.7, 62.8, 71.0, and finally 76.1°C for 2.5, 5, 10, and 15 wt % SiO_2 content, respectively. Furthermore, the intensity of the tan δ peak was lowered for high SiO_2 amounts showing that a portion of the polymer mass could not relax. This is very usual in polymer nanocomposites when strong interactions are taking place.[21] Because of polymer-filler interactions some polymer macromolecules are absorbed on filler surface reducing the mobility of the polymer segments. A transition zone in the matrix is formed surrounding the nanoparticles, which has higher modulus and T_g than the neat polymer. Both properties of the matrix, gradually, reduce with increasing distance from the filler surface. Furthermore, in case the favorable filler–filler interactions are higher than the filler–matrix ones, the nanoparticles tend to form agglomerates. The polymer that is entrapped into these agglomerates also shows higher T_g than the neat polymer. This is an additional reason for T_g increase. In general, this behavior proves that SiO_2 interacts quite strongly with the reactive groups of the polymer, as was verified by FTIR measurements, and restricts the motion of the PVA macromolecules. Hydrogen bonds formed between fumed silica and PVA act as physical crosslinks. As was reported in a recent study, some crosslinks can be generated by heating PVA and silica nanoparticles at elevated temperatures.[22] Such a possibility should not be totally excluded for such samples, albeit insoluble content was negligible in the case of PVA composites of this work.

DSC measurements also showed a slight increase of the melting point of PVA with increasing the SiO_2 content, similar to what was observed for the T_g (Table I). PVA has a melting point $T_m = 226$°C, which for the bionanocomposites containing 10 and 15 wt % SiO_2 increased to 228 and 229°C, respectively. Such an increase in T_m is usual for polymer nanocomposites, because nanoparticles can act as nucleating agents of crystallizable polymers, often leading to the formation of more perfect crystalline structures.[4] In the present PVA/SiO_2 samples, it seems that more perfect crystals are formed.

A shift of the tan δ peak corresponding to the glass transition to higher temperatures was also observed for the Chi/SiO_2 nanocomposites (Fig. 5). The recorded T_g of neat chitosan was 137°C, as can be seen from the tan δ curves, very close to the

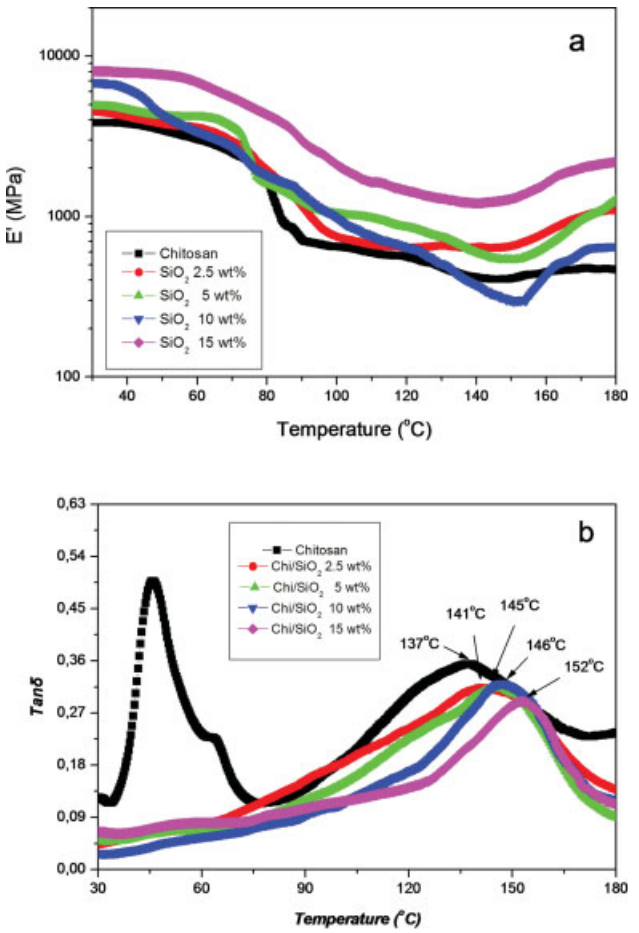

Figure 5 Variation of tan δ for chitosan/SiO_2 nanocomposites containing different SiO_2 content. (a) Storage modulus and (b) tan δ. [Color figure can be viewed in the online issue, which is available at www.interscience.wiley.com.]

values reported in literature.[23] However, it should be mentioned that there is a discrepancy among the reported values for the T_g of chitosan, because various techniques have been used.[24] Differences among samples usually have to do with the deacetylation degree, molecular mass, and degree of crystallinity.[25] In the Chi/SiO_2 nanocomposites of this work, the T_g progressively shifted to higher temperatures by increasing the silica content. Thus, for the sample containing 2.5 wt % SiO_2 the observed T_g was 141°C, whereas for the sample containing 15 wt % SiO_2 the highest T_g value of 152°C was measured. Two factors might be responsible for this behavior. The first is the formation of an interphase surrounding the filler nanoparticles, where macromolecules might be entrapped. Such macromolecules show limited segmental motion. The second is the physical crosslinking. In the case of Chi/SiO_2 nanocomposites, crosslinked macromolecules can be formed because of sufficient interactions of the amine groups of chitosan and the hydroxyl groups of SiO_2.

Except of glass transition, an additional strong peak can be observed in tan δ of neat chitosan in the range between 30 and 80°C. This is the characteristic in chitosan samples with different deacetylation degrees conditioned at environmental humidity and is attributed to structural reorganization of packing of chitosan because of an increase of residual water mobility.[26,27] The intensity of this peak is drastically reduced in the samples containing SiO_2 and moved to slightly higher temperatures. This is evidence that the reorganization ability of chitosan matrix has been reduced, because the matrix became stiffer due to the presence of silica nanoparticles. Furthermore, the formation of crosslinkings between macromolecules because of the interactions of chitosan and SiO_2 has also an additional effect.

The occurrence of crosslinked macromolecules was verified by dissolution measurements of the dried Chi/SiO_2 nanocomposites. For all nanocomposites, significant insoluble content was found after dissolving in water containing 2 wt % acetic acid. In contrast, neat chitosan was completely soluble in the same solvent. To be sure about the insoluble content, the solvent containing the Chi/SiO_2 films was heated at 60°C for 6 h. As can be seen in Figure 6, the insoluble content increased with increasing the SiO_2 content. As a matter of fact, for the sample with 15 wt % of SiO_2 content almost half of the chitosan amount remained insoluble.

This insoluble content is a proof that the interactions between the amide groups of chitosan and surface hydroxyl groups of SiO_2 are very strong leading to the formation of covalent bonds (Fig. 7). This is because the hydroxyl groups of SiO_2 have an acidic nature. In our previous study, similar interactions were also observed between the hydroxyl groups of poly(ethylene terephthalate) and the hydroxyl groups of SiO_2, finally leading to the formation of crosslinked macromolecules.[10]

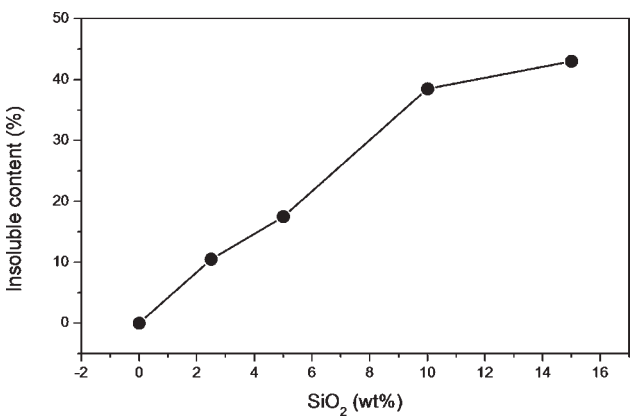

Figure 6 Insoluble content of Chi/SiO2 nanocomposites as a function of silica content.

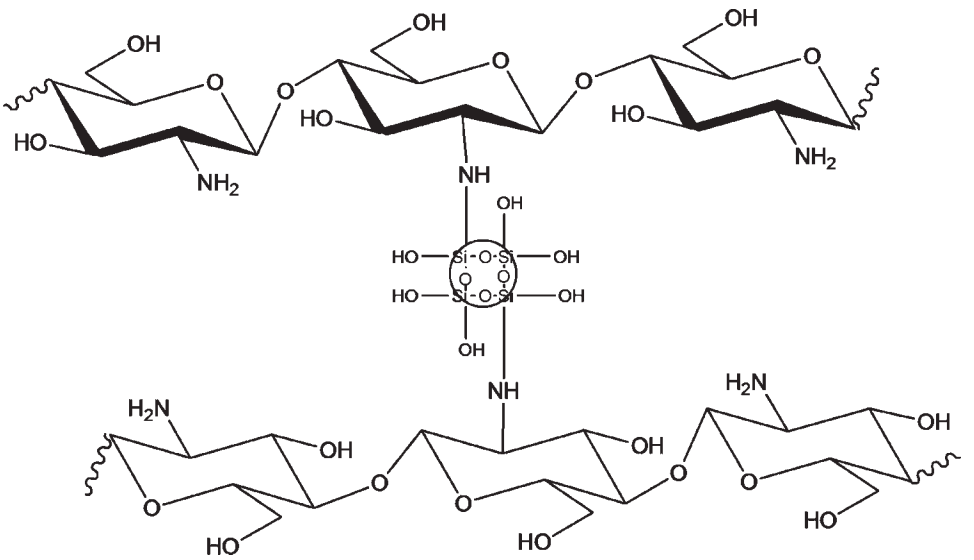

Figure 7 Formation of covalent bond between the amine groups of chitosan and hydroxyl groups of SiO2 leading to crosslinked macromolecules.

PVP/SiO_2 nanocomposites containing different amounts of fumed SiO_2 were transparent. This is an indication that nanoparticles are finely dispersed in the polymer matrix. Unfortunately, fine dispersion of the nanoparticles is not always enough for the resulting composites to achieve sufficient mechanical properties. As has already been mentioned the PVP/SiO_2 nanocomposites, even at high silica loading (15 wt %), remained very brittle and thus it was not possible to measure their tensile properties. However, results of DMA evidenced some enhancement of the matrix for these nanocomposites. As can be seen in Figure 8, with increasing the incorporated amount of silica nanoparticles the materials became stiffer, as the storage modulus for all nanocomposites was much higher than that of the neat PVP. However, as can be seen from tan δ curves, there was a shift of only 1–2°C of T_g to higher temperatures. Similar values were also recorded from DSC thermograms (Table I). This T_g increase compared with the aforementioned for Chi/SiO_2 nanocomposites is very small, indicating that the evolved interactions are rather very weak in this case. This is in full agreement with the conclusions derived from the FTIR study. As a matter of fact, in the case of PVP/SiO_2 bionanocomposites, the T_g for all samples ranged between 165 and 167°C being essentially the same with the T_g of neat PVP. Similar to what was found for PVP/SiO_2 bionanocomposites in a recent study on polyurethane/silica nanocomposites, the T_g was found to be unaffected by the silica content or the silica treatment, as the evolved interactions were also weak.[28]

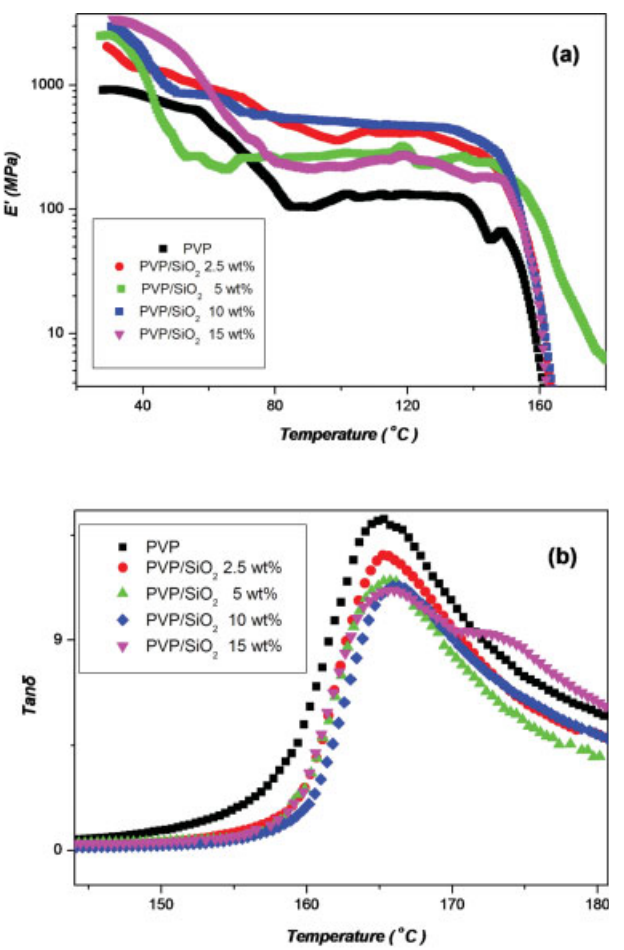

Figure 8 Dynamic mechanical scans of PVP/SiO_2 nanocomposites as function of temperature (a) storage modulus and (b) tan δ. [Color figure can be viewed in the online issue, which is available at www.interscience.wiley.com.]

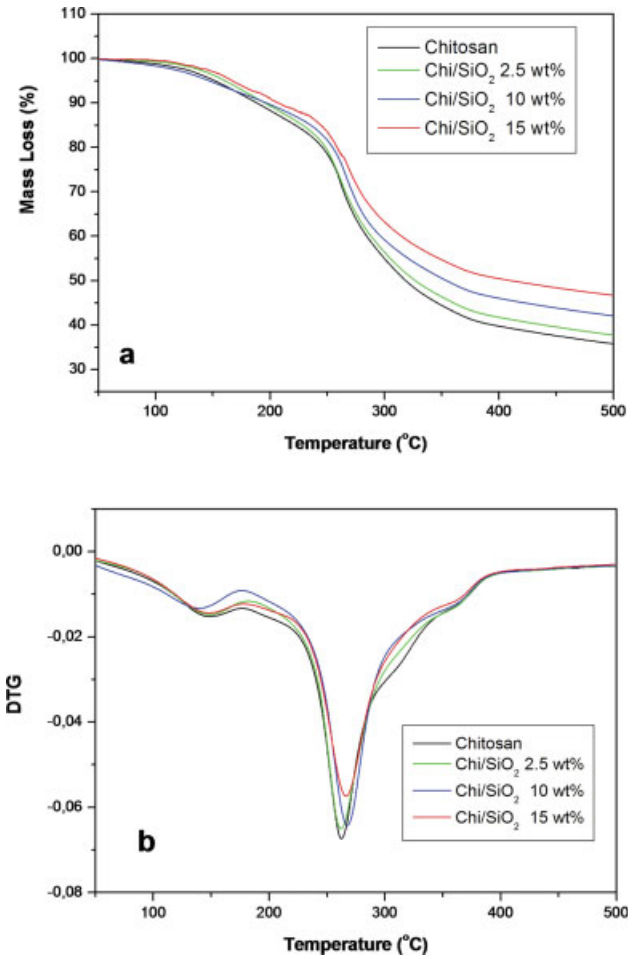

Figure 9 (a) Mass loss (TG%) and (b) derivative mass loss (DTG) versus temperature of chitosan/SiO_2 nanocomposites with heating rate $\beta = 10°C/min$. [Color figure can be viewed in the online issue, which is available at www.interscience.wiley.com.]

Thermogravimetric analysis

One of the major advantages of use of nanoparticles is that they can increase the thermal stability of the polymer matrices that are embedded.[12,29,30] To examine this possibility, the thermal stability of bionanocomposites was investigated by TGA. Tests involved heating scans at a rate of 10°C/min under nitrogen flow. In Figure 9, the mass loss (TG curve) and the derivative mass loss (DTG curve) of neat chitosan and Chi/SiO_2 bionanocomposites are presented. As can be seen, neat chitosan degrades in three well-distinguished steps, which are more obvious in the DTG curves. The first step recorded at the temperature range 100–180°C, corresponding to a mass loss of 8–10 wt %, is associated with the loss of water, whereas the second step, which is the main decomposition step (mass loss 50–55 wt %), is recorded at the temperature range 180–340°C and corresponds to the degradation of chitosan. The third step takes place mainly at the temperature range 340–410°C. It corresponded to a very small mass loss (5–10 wt %) and was associated with chitosan deacetylation.

A similar decomposition mechanism with neat chitosan is also observed for the Chi/SiO_2 bionanocomposites, which also degrade in three steps. However, the temperature corresponding to the maximum decomposition rate varied with filler content of the nanocomposites. For the chitosan nanocomposites containing 2.5 and 5 wt % of SiO_2, the maximum decomposition rate was observed at the same temperature within experimental error, with that for neat chitosan ($T_{dmax} = 262°C$). A similar behavior was also found in our previous study concerning the degradation mechanism of poly(ε-caprolactone)/SiO_2 nanocomposites.[12] However, a remarkable shift of the respective temperature (T_{dmax}) to higher values appeared for nanocomposites containing 10 and 15 wt % SiO_2, as T_{dmax} was 266 and 268°C, respectively. This is an indication that the addition of silica nanoparticles at such a high amount promotes chitosan stabilization against thermal degradation. This is probably because of the shielding effect of the fumed silica nanoparticles. Furthermore, as can be seen from the mass loss (TG) curves, the residue progressively increases, because SiO_2 is not degraded at such low temperatures. Activation energy can be easily calculated from these curves[31–34] but is out of the aims of this study.

Thermal degradation of PVP/SiO_2 nanocomposites was also studied. Figure 10 shows the mass loss (TG) and the derivative mass loss (DTG) curves at heating at a rate 10°C/min for all nanocomposites in comparison with neat PVP. In both thermograms two stages of mass loss can be observed. The first one is taking place at low temperatures (up to 200°C) where the absorbed water from PVP is evaporated. This mass loss corresponds to about 5 wt % of the initial weight. The second mass loss, which corresponds to the main decomposition stage of PVP, takes place at temperatures up to 450°C, where about 90 wt % of the polymer is lost. The temperature at which the maximum decomposition rate is observed was 436°C. From the TG curve, it can be seen that PVP presents a relatively good stability against thermal degradation, because no significant weight loss occurred up to 300°C, ignoring the water loss. A temperature $T_d(-2$ wt %), at which 2.0 wt % of the neat PVP sample has already been thermally degraded and lost, was hereby taken as index to express its thermal stability. This temperature is close to 320°C.

The thermal behavior of PVP/SiO_2 nanocomposites was very similar with that discussed for neat PVP, with the most significant difference being in the amount of the residue, as was expected. Because SiO_2 is not degraded at such low temperatures by

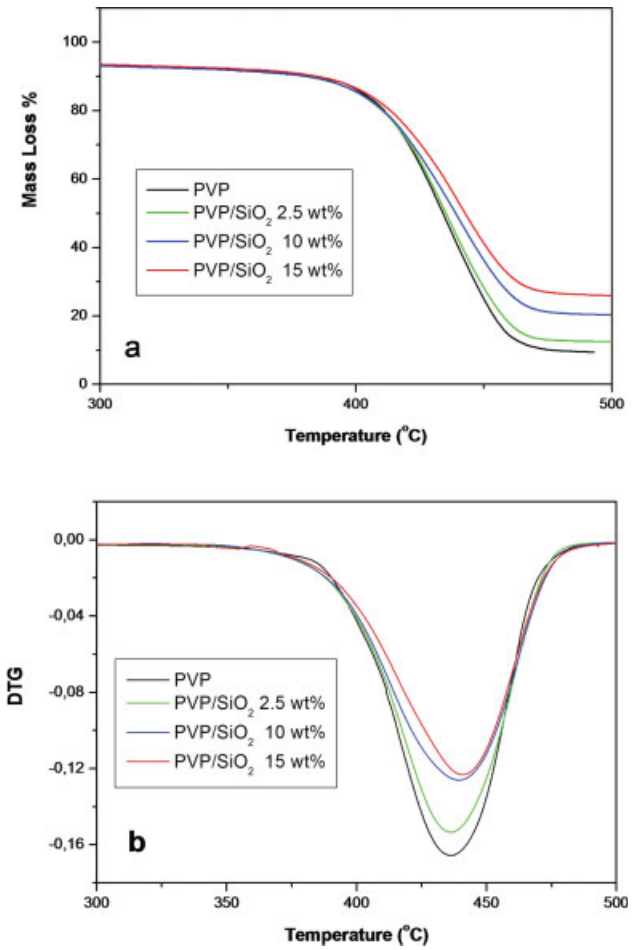

Figure 10 (a) Mass loss (TG%) and (b) derivative mass loss (DTG) versus temperature for PVP/SiO_2 nanocomposites with heating rate $\beta = 10^{\circ}C/min$. [Color figure can be viewed in the online issue, which is available at www.interscience.wiley.com.]

increasing its content in the PVP matrix, the percentage of the residue increases proportionally to the added amount of SiO_2. Careful examination of the DTG curves, focusing on the main decomposition stage, shows that the temperature corresponding to the maximum rate of decomposition increases slightly. Thus, for nanocomposites containing 10 and 15 wt % these temperatures were 439 and 441°C, respectively, whereas for nanocomposites containing lower SiO_2 content the increase comparing with neat PVP was only 1°C. This shift reveals that incorporation of SiO_2 can increase the thermal stability of PVP, as is always observed in nanocomposites. It is well known that when inorganic filler particles are dispersed in a polymer matrix, the formed layers are impermeable toward small molecules -gases or volatile liquids- that are generated during decomposition and a much longer path around the nanoparticles is needed for their removal from the decomposed matrix.

Thermal stability of PVA nanocomposites is of special interest. Recently, PVA/SiO_2 membranes have gained increasing interest for fuel cell applications, because the incorporation of silica particles in the PVA matrix reduces the free water ratio of the membranes and results in a remarkable reduction of methanol permeability.[35–37] Commercial poly(vinyl alcohol) (PVA) is a hydrophilic polymer containing pendant hydroxyl groups. It cannot be prepared by the direct polymerization of vinyl alcohol and thus it is derived from the hydrolysis of poly(vinyl acetate) (PVAc). The thermal degradation behavior of PVA and its bionanocomposites was examined with TGA, and the recorded thermograms are shown in Figure 11. According to the DTG curves, three degradation steps could be observed apart from the one that takes place at temperatures below 150°C and which is due to evaporation of absorbed water (about 3 wt % mass loss). The weight loss in the first and second stages, with maximum decomposition rate temperatures 280 and 310°C, respectively, could be

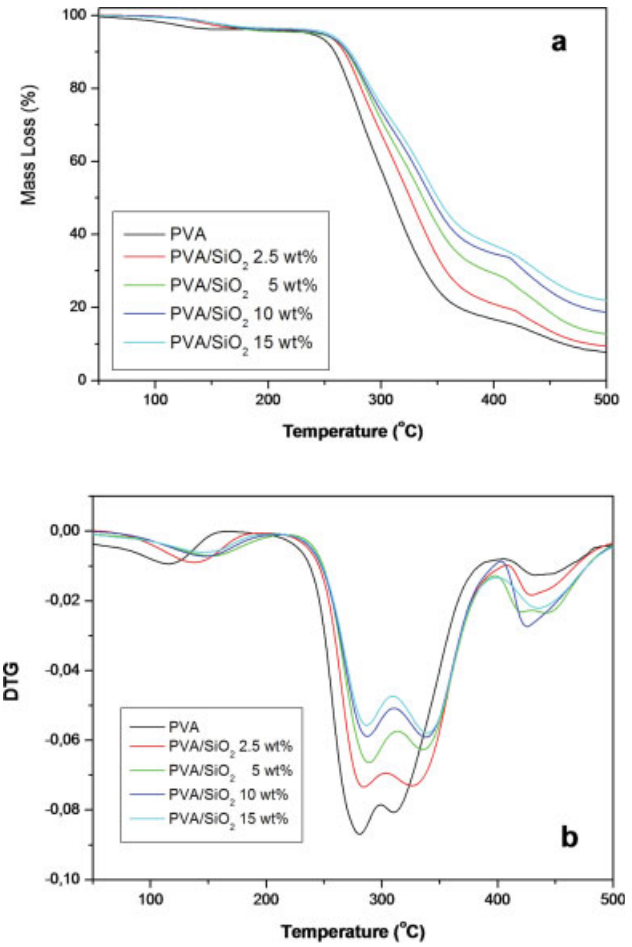

Figure 11 (a) Mass loss (TG) and (b) derivative mass loss (DTG) versus temperature of PVP/SiO_2 nanocomposites with heating rate $\beta = 10^{\circ}C/min$. [Color figure can be viewed in the online issue, which is available at www.interscience.wiley.com.]

attributed to the decomposition of the PVA by a dehydration reaction on the polymer chain and degradation of main backbones. The weight loss corresponding to the first stage is ~ 35–36%, whereas the theoretical value for the complete dehydration is 38.6%. It is worth noting that this decomposition temperature is shifted by about 5–10°C to higher temperatures with increase of the silica content, which means that the dehydration process is hindered. A similar stabilization, because of SiO_2 nanoparticles was also reported by Etienne et al., who studied PMMA/SiO_2 nanocomposites.[38] This could be attributed to interactions taking place between the hydroxyl groups of PVA and the surface hydroxyl groups of SiO_2 proven by FTIR spectroscopy. In the third weight loss process with a maximum decomposition temperature 430°C, the degradation of the polyene residues takes place. At last, the amount of the residue depends on the silica content.

From all the earlier TGA study, it became clear that the addition of SiO_2 nanoparticles enhances the thermal stability of the polymer matrices.

CONCLUSIONS

The addition of fumed silica nanoparticles into different biocompatible polymer matrices resulted in the formation of biocompatible nanocomposites with enhanced mechanical and thermal properties. The extent of this enhancement depends mainly on the evolved interactions between the functional groups of the polymers and surface hydroxyl groups of SiO_2. All nanocomposites are more stable against thermal degradation than the neat polymers. FTIR measurements verified sufficient interactions of SiO_2 with the reactive groups of PVA and chitosan. Filler/matrix interactions resulted in restriction in the segmental motion of the matrix macromolecules. Indeed, DMA proved that the glass transition of these polymers progressively shifted to higher temperatures with increasing the silica content, and also showed that a portion of the polymer matrix mass of the nanocomposites did not contribute to the a-relaxation.

References

1. Tjong, S. C. Mater Sci Eng 2006, 653, 73.
2. Moniruzzaman, M.; Winey, K. I. Macromolecules 2006, 39, 5194.
3. Usuki, A.; Hasegawa, N.; Kato, M. Adv Polym Sci 2005, 179, 135.
4. Papageorgiou, G. Z.; Achilias, D. S.; Bikiaris, D. N.; Karayannidis, G. P. Thermochim Acta 2005, 427, 117.
5. Bikiaris, D. N.; Vassiliou, A.; Pavlidou, E.; Karayannidis, G. P. Eur Polym Mater 1965, 2005, 41.
6. Pavlidou, E.; Bikiaris, D.; Vassiliou, A.; Chiotelli, M.; Karayannidis, G. J Phys Conf Ser 2005, 10, 190.
7. Bikiaris, D. N.; Papageorgiou, G. Z.; Pavlidou, E.; Vouroutzis, N.; Palatzoglou, P.; Karayannidis, G. P. J Appl Polym Sci 2006, 100, 2684.
8. Vladimirov, V.; Betchev, C.; Vassiliou, A.; Papageorgiou, G.; Bikiaris, D. Comp Sci Technol 2006, 66, 2935.
9. Vassiliou, A.; Papageorgiou, G. Z.; Achilias, D. S.; Bikiaris, D. N. Macromol Chem Phys 2007, 21, 364.
10. Bikiaris, D.; Karavelidis, V.; Karayannidis, G. P. Makromol Rapid Commun 2006, 27, 1199.
11. Chrissafis, K.; Antoniadis, G.; Paraskevopoulos, K. M.; Vassiliou, A.; Bikiaris, D. N. Comp Sci Technol 2007, 67, 2165.
12. Vassiliou, A.; Bikiaris, D. N.; Pavlidou, E. Macromol React Eng 2007, 1, 488.
13. Oriakhi, C. O. J Chem Educ 2000, 77, 1138.
14. Hassan, C. M.; Peppas, N. A. Adv Polym Sci 2000, 153, 37.
15. Friedrich, H.; Fussnegger, B.; Kolter, K.; Bodmeier, B. Eur J Pharm Biopharm 2006, 62, 171.
16. Watanabe, T.; Hasegawa, S.; Wakiyama, N.; Kusai, A.; Senna, M. Int J Pharm 2003, 250, 283.
17. Gun'ko, V. M.; Voronin, E. F.; Zarko, V. I.; Goncharuk, E. V.; Turov, V. V.; Pakhovchishin, S. V.; Pakhlov, E. M.; Guzenko, N. V.; Leboda, R.; Skubiszewska-Zieba, J.; Janusz, W.; Chibowski, S.; Chibowski, E.; Chuiko, A. A. Colloid Surf A 2004, 233, 63.
18. Gun'ko, V. M.; Zarko, V. I.; Voronin, E. F.; Turov, V. V.; Mironyuk, I. F.; Gerashchenko, I. I.; Goncharuk, E. V.; Pakhlov, E. M.; Guzenko, N. V.; Leboda, R.; Skubiszewska-Zieba, J.; Janusz, W.; Chibowski, S.; Levchuk, Y. N.; Klyueva, A. V. Langmuir 2002, 18, 581.
19. Mojumdar, S. C.; Raki, L. J Therm Anal Calorim 2005, 82, 89.
20. Lai, S. M.; Yang, A. J.; Chen, W. C.; Hsiao, J. F. Polym Plast Technol Eng 2006, 45, 997.
21. Yang, D. Z.; Liu, Q. X.; Xie, X. L.; Zeng, F. D. J Therm Anal Calorim 2006, 84, 355.
22. Bondyopadhyay, A.; Bhowmick, A. K. Plast Rubber Compos 2006, 35, 210.
23. Dong, Y.; Ruan, Y.; Wang, H.; Zhao, Y.; Bi, D. J Appl Polym Sci 2004, 93, 1553.
24. Lazaridou, A.; Biliaderis, C. G. Carbohydr Polym 2002, 48, 179.
25. Estrela dos Santos, J.; Dockal, E. R.; Cavalheiro, E. T. G. J Therm Anal Calorim 2005, 79, 243.
26. Mano, J. F. Macromol Biosci 2008, 8, 69.
27. Mucha, M.; Pawlak, A. Thermochim Acta 2005, 427, 69.
28. González-Irún Rodríguez, J.; Carreira, P.; García-Diez, A.; Hui, D.; Artiaga, R.; Liz-Marzán, L. M. J Therm Anal Calorim 2007, 87, 45.
29. Marosfői, B. B.; Szabó, A.; Marosi, G.; Tabuani, D.; Camino, G.; Pagliari, S. J Therm Anal Calorim 2006, 86, 669.
30. Araújo, E. M.; Barbosa, R.; Oliveira, A. D.; Morais, C. R. S.; de Mélo, T. J. A.; Souza, A. G. J Therm Anal Calorim 2007, 87, 811.
31. Vyazovkin, S. J Comput Chem 2001, 22, 178.
32. Peterson, J. D.; Vyazovkin, S.; Wight, C. A. Macromol Chem Phys 2001, 202, 775.
33. Vyazovkin, S.; Sbirrazzuoli, N. Macromol Rapid Commun 2006, 27, 1515.
34. Chrissafis, K.; Paraskevopoulos, K. M.; Bikiaris, D. N. Polym Degrad Stab 2006, 91, 60.
35. Kim, D. S.; Park, H. B.; Rhim, J. W.; Lee, Y. M. J Membr Sci 2004, 240, 37.
36. Panero, S.; Fiorenza, P.; Navarra, M. A.; Romanowska, J.; Scrosati, S. J Electrochem Soc 2005, 152, A2400.
37. Libby, B.; Smyrl, W. H.; Cussler, E. L. AIChE J 2003, 49, 991.
38. Etienne, S.; Becker, C.; Ruch, D.; Grignard, B.; Cartigny, G.; Detrembleur, C.; Calberg, C.; Jerome, R. J Therm Anal Calorim 2007, 87, 101.